Dalton Transactions

Accepted Manuscript

ROYAL SOCIETY OF CHEMISTRY

www.rsc.org/dalton

Exploring the effect of the Ln^{III}/Ln^{II} redox potential on C–F activation and on oxidation of some lanthanoid organoamides

Glen. B. Deacon,[a*] Peter C. Junk,[b*] Rory P. Kelly[a] and Jun Wang[a, b]

[a]School of Chemistry, Monash University, Clayton 3800, Australia.

[b]College of Science, Technology & Engineering, James Cook University, Townsville 4811, Qld, Australia.

[*]Corresponding authors: glen.deacon@monash.edu; peter.junk@jcu.edu.au

Abstract

The divalent europium complexes, $[Eu(L^{Me/Et})_2(thf)_2]$ and $[Eu(L^{Et})_2(dme)]$ ($L^{Me/Et}$ = *p*-$HC_6F_4N(CH_2)_2NMe_2/Et_2$), have been prepared from redox-transmetallation/protolysis (RTP) reactions between Eu metal, $Hg(C_6F_5)_2$ and $L^{Me/Et}H$ in thf. The complexes exhibit close (C)F–Ln interactions and the amide ligands feature tridentate *N,N',F* chelation. The complexes are thermally robust but on exposure to light they undergo C–F activation. From exposure of $[Eu(L^{Et})_2(thf)_2]$ to light, the Eu^{III} mixed fluoride/oxide cluster, $[Eu_4(L^{Et})_6F_2O_2]$ was isolated, but other well-defined C–F activation products have proven elusive due to the stability of Eu^{II}. Oxidation of $[Ln(L^R)_2(thf)_2]$ (Ln = Eu, R = Me; Ln = Yb, R = Et) with I_2 afforded the heteroleptic iodo complexes, $[Ln(L^R)_2I(thf)_n]$ (Ln = Eu, n = 1; Ln = Yb, n = 0), and the homoleptic complexes, $[Ln(L^R)_3]$. The formation of the iodo complexes and the heteroleptic complexes appear to occur by different routes. $[Yb(L^{Et})_3]$ shows interesting structural differences from reported $[Ln(L^{Et})_3]$ (Ln = La, Ce, Nd) complexes, and highlights an incomplete shift towards *N,N'* chelation to the much smaller Yb ion. $[Sm(L^{Me})_3]$ was prepared from a protolysis reaction between $[Sm(CH_2C_6H_4\text{-}NMe_2\text{-}o)_3]$ and $L^{Me}H$. Heating a solution of $[Sm(L^{Me})_3]$ in toluene at 110 °C for three days did not afford any samarium fluoride complex. An RTP reaction with Sm afforded the heteroleptic samarium complex, $[Sm(L^{Me})_2F]_3$, in very low yield. From an attempted protolysis reaction between $[Sm(DippForm)_2(thf)_2]$ and $L^{Me}H$, the mixed ligand samarium fluoride complex, $[Sm(DippForm)(L^{Me})F]_2$, was isolated. Overall, the instability of Sm^{II} precludes control over the C–F activation reactions.

Introduction

As a consequence of the high strength of rare earth–fluorine bonds,[1] rare earth compounds have the capacity to effect C–F activation, which is preceded by (C)–F–Ln binding.[2, 3] In order to optimise the likelihood of activation, an attractive strategy is to use a donor atom (C, N, O, S) to anchor a fluorocarbon group to a rare earth metal in a position where (C)–F–Ln binding is possible in a Ln–D–$(C)_nF$ (D = C, N, O, S; n = 1–3) four to six-membered chelate ring. To this end, we have utilised *N,N*-dialkyl-*N'*-2,3,5,6-tetrafluorophenylethane-1,2-diamines (Fig. 1), which on deprotonation anchor the rare earth metal through *N,N'*-chelation in a position where (C)–F–Ln binding is possible as part of a five-membered ring.[4-14] Using this strategy, $[Yb(L^{Me,Et})_2(thf)_2]$ complexes were prepared by metathesis, by protolysis of $[Yb\{N(SiMe_3)_2\}_2(thf)_2]$ with $L^{Me,Et}H$, and by redox transmetallation/protolysis (RTP) between Yb metal, $Hg(C_6F_5)_2$ and $L^{Me,Et}H$.[14] These complexes were shown to have Yb–F–C(Ar) bonding interactions in solution by ^{19}F and ^{171}Yb NMR data, and the X-ray crystal structure of the dme analogue $[Yb(L^{Et})_2(dme)]$ (dme = 1,2-dimethoxyethane) involved Yb–F–C(Ar) bonding. The complexes underwent C–F activation to give $[Yb^{III}_4(L^{Me,Et})_6F_6]$ cages in good yields. The importance of the Ln^{II} oxidation state in promoting C–F activation reactions became evident in a study of the homoleptic Ln^{III} complexes $[Ln(L^{Me,Et})_3]$ (Ln = La, Ce, Nd), which have two tridentate *N,N',F* ligands and one bidentate *N,N'* (L^{Me}) or *N,F* (L^{Et}) ligand (the *N,N',F* binding mode is depicted in Fig. 1).[13] These complexes of elements without a readily accessible Ln^{II} state (although Ln^{II} complexes of these elements are known[15-21]) gave only low yields of $[Ln(L^{Me})_2F]_3$ (Ln = La, Ce) or $[Nd(L^{Et})_2F]_2$ during their preparation by RTP. Heating $[Ln(L^{Me})_3]$ gave $[Ln(L^{Me})_2F]_3$ for Ln = Ce but not Ln = La. We have also studied the redox-inert group 2 complexes, $[Mg(L^R)_2]$ and $[Ca(L^R)_2(thf)_2]$, and found that they do not undergo C–F activation, even under forcing conditions.[22] The contrast between the behaviour of Yb on the one hand, and La, Ce and Nd on the other, has led us to examine the role of the Ln^{III}/Ln^{II} oxidation potential on the occurrence of C–F activation. Thus, we have now examined the Ln/$Hg(C_6F_5)_2$/L^RH reactions for Sm and Eu, where the Ln^{II} oxidation state is less and more stable respectively than Yb^{II} and report the synthesis and structures of $[Sm(L^{Me})_3]$, $[Sm(L^{Me})_2F]_3$ and $[Sm(DippForm)(L^{Me})F]_2$ complexes, and the synthesis and stability of $[Eu(L^{Me,Et})_2(solv)_2]$ (solv = thf or ½ dme) complexes. Isolable heteroleptic lanthanoid fluoride species, $[LnL_2F]_n$,[23, 24] are still a rarity, though more are being prepared, whilst structurally characterised $[LnLF_2]$ species are not known, even though some complexes with higher F:Ln ratios than 2:1 have been prepared.[25]

Rearrangement into highly insoluble LnF_3 is always a potential issue. Of note, is the isolation of the first divalent[26] and tetravalent[27] heteroleptic lanthanoid fluoride complexes. In addition, we have compared the reactivity of $[Eu(L^{Me})_2(thf)_2]$ and $[Yb(L^{Et})_2(thf)_2]$ in oxidation reactions with iodine, where not only are $[Ln(L^{Me,Et})_2I]$ complexes obtained but also homoleptic $[Ln(L^{Me,Et})_3]$ complexes. Moreover, the structure of $[Yb(L^{Et})_3]$ shows unexpected features compared with the reported structures of $[Ln(L^{Et})_3]$ (Ln = La, Ce, Nd).[13]

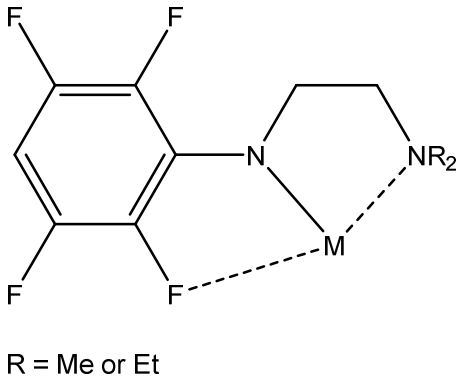

Fig. 1 Possible binding mode of *p*-$HC_6F_4N(CH_2)_2NR_2(1-)$ (L^R, R = Me or Et) ligands

Results and Discussion

Syntheses

The bright yellow divalent europium complexes **$[Eu(L^{Me})_2(thf)_2]$** and **$[Eu(L^{Et})_2(thf)_2]$** were synthesised in reasonable yields by redox-transmetallation/protolysis (RTP) reactions in thf between europium metal, $Hg(C_6F_5)_2$ and two equivalents of $L^{Me}H$ or $L^{Et}H$ respectively. Recrystallisation of **$[Eu(L^{Et})_2(thf)_2]$** from dme yielded bright yellow **$[Eu(L^{Et})_2(dme)]$**. Unlike the analogous ytterbium complexes, the europium complexes are thermally stable and if shielded from light they are robust. However, when they are exposed to light they turn a dark red/purple colour both in solution and in the solid state. Unsurprisingly, the transformation is much slower in the solid state than in solution. Unfortunately, this decomposition is complex, and **$[Eu_4(L^{Et})_6F_2O_2]$** is the only identifiable product that has been isolated to date. The oxygen atoms are plausibly derived from adventitious oxygen or cleavage of thf. The formation of these crystals was accompanied by dark red/purple plates, which only diffracted very poorly. These crystals were obtained on multiple occasions but we were unable to obtain a solvable data set.

When samarium metal, $Hg(C_6F_5)_2$ and two equivalents of $L^{Me}H$ were stirred in thf for several days, a large amount of a poorly soluble dark brown solid was obtained. A small number of single crystals of **[Sm(L^{Me})$_2$F]$_3$**·1.5PhMe were isolated from the filtered reaction mixture, but the very low yield prevented further characterisation. Although the above reactions (summarised in Scheme 1) only yielded very minor amounts of C–F activation products, when compared with the results obtained using ytterbium, important insights into the mechanism of C–F activation mediated by oxidation state have been obtained (*vide infra*).

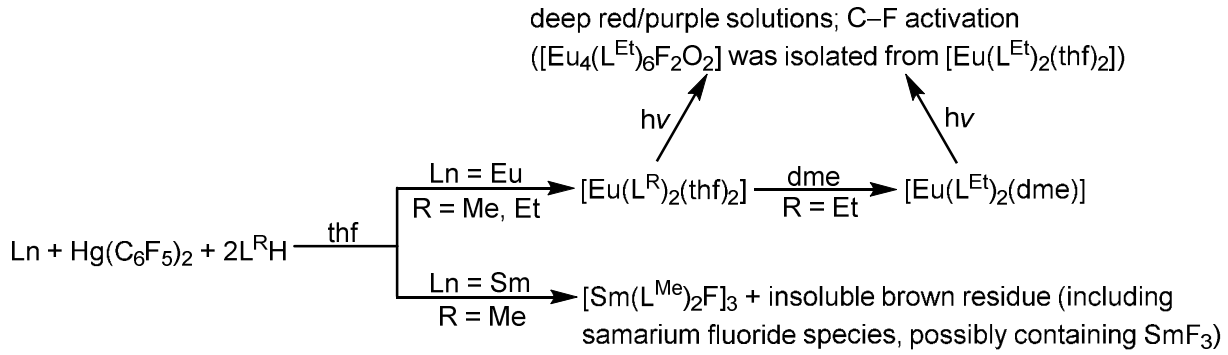

Scheme 1 Syntheses of $[Eu(L^R)_2(thf)_2]$, **[Eu(L^{Et})$_2$(dme)]** and **[Sm(L^{Me})$_2$F]$_3$**.

In addition, the homoleptic trivalent samarium complex, **[Sm(L^{Me})$_3$]**, was prepared in good yield by treating the samarium benzyl complex $[Sm(CH_2C_6H_4\text{-}NMe_2\text{-}o)_3]$[28] with three equivalents of $L^{Me}H$ in toluene (Equation 1). A solution of **[Sm(L^{Me})$_3$]** in C_7D_8 was heated at 110 °C for three days, but no appreciable transformation of **[Sm(L^{Me})$_3$]** into **[Sm(L^{Me})$_2$F]$_3$** was observed. This rules out **[Sm(L^{Me})$_3$]** as the source of **[Sm(L^{Me})$_2$F]$_3$**, and indicates that Sm^{III} cannot induce C–F activation of L^R ligands.

$$[Sm(CH_2C_6H_4\text{-}NMe_2\text{-}o)_3] + 3L^{Me}H \xrightarrow{PhMe} [Sm(L^{Me})_3] + 3CH_3C_6H_4\text{-}NMe_2\text{-}o \qquad (1)$$

Since RTP did not afford an isolable divalent samarium complex that could then undergo C–F activation, a protolysis reaction between $[Sm(DippForm)_2(thf)_2]$ (DippForm = 2,6-diisopropylphenylformamidinate) and $L^{Me}H$ was attempted in toluene (Equation 2). The reaction is complex, with NMR spectroscopy showing the formation of multiple products, but a few yellow crystals of the dimeric heteroleptic fluoride complex, **[Sm(DippForm)(L^{Me})F]$_2$**·$2C_6H_6$, were isolated. Despite use of an excess of $L^{Me}H$, only monoprotolysis occurred before C–F

activation in the case of the isolated product. The more reducing nature of the Sm^{II} ion relative to the Yb^{II} ion is presumably why a divalent samarium complex was not isolated before C–F activation could occur. Attempts to prepare this complex in bulk failed.

$$[Sm(DippForm)_2] + L^{Me}H \text{ (xs)} \xrightarrow{PhMe} [Sm(DippForm)(L^{Me})F]_2 + HDippForm + \text{other products} \quad (2)$$

We attempted the oxidation of **$[Eu(L^{Me})_2(thf)_2]$** and $[Yb(L^{Et})_2(thf)_2]$ using iodine, and we obtained some slightly unexpected results. The oxidation of **$[Eu(L^{Me})_2(thf)_2]$** resulted in the formation of blue crystals of **$[Eu(L^{Me})_2I(thf)]$** as the major product, and a few bright blue crystals of **$[Eu(L^{Me})_3]$** as a minor product. When the same oxidation reaction was attempted with $[Yb(L^{Et})_2(thf)_2]$, dark red crystals of **$[Yb(L^{Et})_2I]$** were obtained. When the reaction stoichiometry was changed to *ca.* 1:1, red crystals of **$[Yb(L^{Et})_3]$** were isolated. These reactions are summarised in Scheme 2.

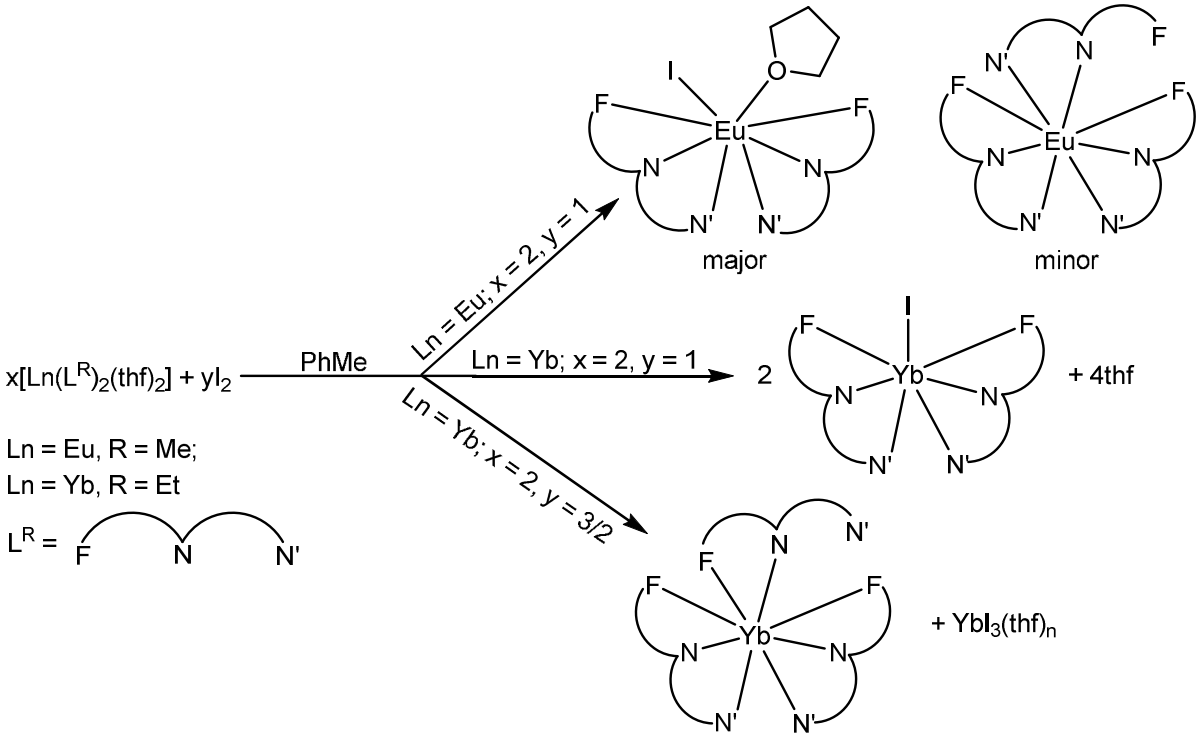

Scheme 2 Oxidation of **$[Eu(L^{Me})_2(thf)_2]$** and $[Yb(L^{Et})_2(thf)_2]$ by iodine.

The formation of the homoleptic complexes, **$[Eu(L^{Me})_3]$** and **$[Yb(L^{Et})_3]$**, could reasonably be expected to arise from rearrangement of **$[Eu(L^{Me})_2I(thf)]$** and **$[Yb(L^{Et})_2I]$** respectively.

However, when **[Yb(L^{Et})$_2$I]** was heated at 70 °C for two days, no transformation into **[Yb(L^{Et})$_3$]** was observed (Equation 3), hence the formation of **[Yb(L^{Et})$_3$]**, and presumably **[Eu(L^{Me})$_3$]**, is a distinct reaction from the formation of [Ln(L^{Et})$_2$I(thf)$_n$] (Ln = Yb, n = 0; Ln = Eu, n = 1) complexes.

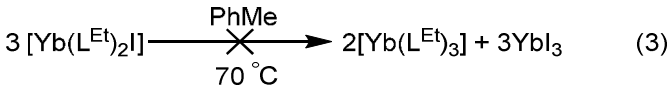

Characterisation

Where possible, all complexes were characterised by standard analytical techniques. No interpretable ^{1}H NMR spectra could be obtained for any of the europium complexes, owing to paramagnetism, although the ^{19}F{^{1}H} NMR spectra of **[Eu(L^{Me})$_2$(thf)$_2$]** and **[Eu(L^{Et})$_2$(dme)]** each show one broad signal at *ca.* −140 ppm and −149 ppm respectively. In the room temperature spectra of paramagnetic cerium L^R complexes, the F3,5 atoms are observed at about −140 ppm but the signals corresponding to the F2,6 atoms are broadened into the baseline. However, obtaining the ^{19}F{^{1}H} NMR spectra of the cerium complexes at higher temperatures allowed for the observation of a very broad signal corresponding to the F2,6 atoms at approximately −180 ppm for [Ce(L^{Me})$_3$], and at about −200 ppm for [Ce(L^{Me})$_2$F]$_3$ and [Ce(L^{Et})$_3$].[13] Unfortunately, this approach was not successful for the divalent europium complexes. On the other hand, the spectrum of **[Eu(L^{Me})$_2$I(thf)]** at 343 K shows a broad singlet at about −139 ppm that is attributable to the F3,5 atoms, and a very broad singlet at −185 ppm that corresponds to the F2,6 atoms. The ^{1}H NMR spectrum of **[Sm(L^{Me})$_3$]** at 333 K is consistent with the solid-state structure, and it only shows modest paramagnetic shifting and broadening due to the paramagnetic Sm^{III} centre. The ^{19}F{^{1}H} NMR spectrum is similar to that of [La(L^{Me})$_3$],[13] and it shows resonances at −143.4 and −164.8 ppm (broad), attributable to the F3,5 and F2,6 atoms respectively. In contrast to the europium complexes, the ytterbium complexes provide interpretable ^{1}H NMR spectra, although elevated temperatures are necessary. The ^{1}H spectrum of **[Yb(L^{Et})$_2$I]** at 343 K shows broad, paramagnetically shifted signals over the range 21.81 to −79.47 ppm. Likewise, broad and paramagnetically shifted peaks are observed for **[Yb(L^{Et})$_3$]** over the range 26.82 to −68.41 ppm. At room temperature, the ^{19}F{^{1}H} NMR spectrum of **[Yb(L^{Et})$_2$I]** only shows one broad singlet at −127.5 ppm, but at 343 K, two broad signals are seen at −35.3 ppm (F2,6) and −130.8 ppm (F3,5). Conversely, the ^{19}F{^{1}H} NMR

spectrum of **[Yb(L^{Et})$_3$]** obtained at 343 K only displays one signal at −134.8 ppm but, obtaining the spectrum at 383 K allowed for the observation of the F2,6 atoms as a very broad singlet at −59.2 ppm, whilst a singlet corresponding to the F3,5 atoms is at −135.8 ppm.

In order to further confirm the bulk identity of the divalent europium samples, each complex was dissolved in CD_3CN and then one drop of trifluoroacetic acid was added to protolyse the L^R ligands in order to compare the ratio of L^RH:thf(dme) (Equation 4). For **[Eu(L^{Me})$_2$(thf)$_2$]**, the L^{Me}H:thf ratio of 1:1 was the same as the solid-state structure, whilst for **[Eu(L^{Et})$_2$(thf)$_2$]**, the L^{Et}H:thf ratio of 1:0.8 was slightly lower than in the solid-state structure, possibly owing to loss on storage or hydrolysis. For **[Eu(L^{Et})$_2$(dme)]**, the L^{Et}H:dme ratio of 2:1 is the same as the solid-state structure.

$$[Eu(L^R)(solv)_2] \xrightarrow[CD_3CN]{CF_3COOH} [Eu(OOCCF_3)_2(NCD_3)_n] + 2L^RH + 2solv \qquad (4)$$

(R = Me, solv = thf; R = Et, solv = thf, $^1/_2$ dme)

Both **[Eu(L^{Me})$_2$I(thf)]** and **[Eu(L^{Me})$_3$]** were also characterised by UV-vis spectroscopy. The absorption maxima for **[Eu(L^{Me})$_2$I(thf)]** (609 nm in the solid state; 613 nm in solution) and **[Eu(L^{Me})$_3$]** (573 nm) are consistent with their blue colours, and the absorptions are presumably a result of ligand-to-metal charge transfer.

The IR spectra of all complexes are similar to those of reported L^R complexes,[13] and they display υ(CF) absorptions between 955–957 cm^{-1} and 921–926 cm^{-1} for the L^{Me} complexes, and between 942–944 cm^{-1} for the L^{Et} complexes. The IR spectrum of the insoluble brown residue isolated from the reaction that yielded **[Sm(L^{Me})$_2$F]$_3$** also shows bands consistent with coordinated L^{Me} ligands, although it is likely that it is a mixture of compounds.

Microanalysis results for **[Yb(L^{Et})$_2$I]** and **[Sm(L^{Me})$_3$]** are in excellent agreement with the single crystal compositions. The results for **[Eu(L^{Me})$_2$I(thf)]** indicate the loss of 50 % of the coordinated thf. Samples of **[Sm(L^{Me})$_2$F]$_3$**, **[Eu(L^{Et})$_2$(dme)]** and **[Eu(L^{Et})$_2$(dme)]** were also sent for microanalysis but the results were poor. The results for **[Sm(L^{Me})$_2$F]$_3$** were extremely low in C, H and N, thus indicating a large amount of inorganic material, presumably samarium fluoride and related species. The poor results for the divalent europium complexes are possibly due to C–F activation of the samples in the solid state during transport overseas for analysis.

Consequently, **[Eu(L^{Me})$_2$(thf)$_2$]**, **[Eu(L^{Et})$_2$(thf)$_2$]** and **[Eu(L^{Et})$_2$(dme)]** were analysed for europium content by complexometric titration after acid digestion of the samples[29, 30] giving satisfactory results. **[Yb(L^{Et})$_3$]** was characterised by an Yb analysis, and the result was in good agreement with the crystal composition. Since only small amounts of **[Sm(DippForm)(L^{Me})F]$_2$**, **[Sm(L^{Me})$_2$F]$_3$**, **[Eu$_4$(L^{Et})$_6$F$_2$O$_2$]** and **[Eu(L^{Me})$_3$]** were isolated, no microanalytical data could be obtained for these complexes.

Molecular structures

Structures of the divalent europium complexes

The molecular structures of **[Eu(L^{Me})$_2$(thf)$_2$]**, **[Eu(L^{Et})$_2$(thf)$_2$]** and **[Eu(L^{Et})$_2$(dme)]** (isosmorphous with [Yb(L^{Et})$_2$(dme)])[14] are all very similar. Given that single crystals were not obtained for [Yb(L^{Me})$_2$(thf)$_2$] and [Yb(L^{Et})$_2$(thf)$_2$],[14] the structures of **[Eu(L^{Me})$_2$(thf)$_2$]** and **[Eu(L^{Et})$_2$(thf)$_2$]** most likely serve as good representations of the ytterbium compounds, especially given [Ln(L^{Et})$_2$(dme)] (Ln = Eu, Yb) are isomorphous. The representative structure of **[Eu(L^{Me})$_2$(thf)$_2$]** is shown in Fig. 2, and selected bond lengths for each complex are listed in Table 1, along with those of [Yb(L^{Et})$_2$(dme)] for comparison. All of the europium complexes are eight-coordinate and they feature two *N,N′,F*-chelating L^R ligands and two coordinating thf or dme oxygen atoms. The complexes are notable for the presence of short Eu–F(C) interactions, which are shorter than the corresponding Eu–NR$_2$ bond lengths (Table 1). The Eu–F(C) bond lengths (**[Eu(L^{Et})$_2$(dme)]** (2.630(2)–2.632(2) Å) < **[Eu(L^{Me})$_2$(thf)$_2$]** (2.656(2)–2.680(2) Å), < **[Eu(L^{Et})$_2$(thf)$_2$]** (2.679(10)–2.683(10) Å) are much shorter than the only other europium complexes with Eu–F(C) bonding interactions, namely the divalent perfluorophenolate complex, [Eu$_3$(OC$_6$F$_5$)$_6$(dme)$_4$] (2.928(2)–3.013(2) Å),[7] the mixed oxidation state perfluorophenolate complex, [Eu$_2$(OC$_6$F$_5$)$_5$(dme)$_3$] (2.796(4)–3.109(5) Å),[7] and [Eu(μ-SC$_6$F$_5$)$_2$(thf)$_2$]$_n$ (3.006(6) Å).[5]

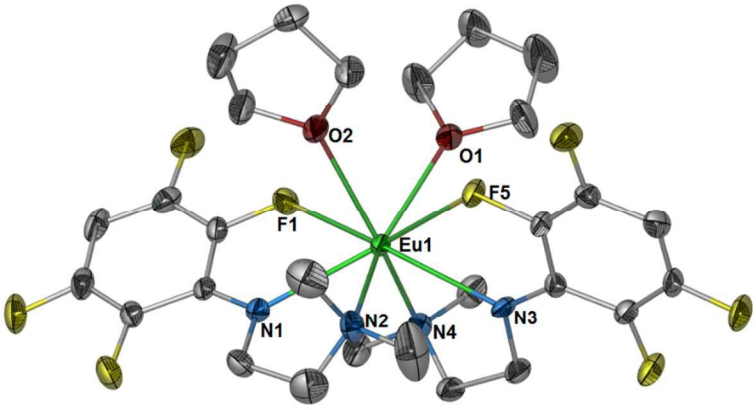

Fig. 2 Molecular structure of **[Eu(L^{Me})$_2$(thf)$_2$]** shown with 50 % probability thermal ellipsoids; hydrogen atoms have been omitted for clarity.

Table 1 Selected bond lengths (Å) for [Eu(*p*-HC$_6$F$_4$N(CH$_2$)$_2$NMe$_2$)$_2$(thf)$_2$] (**[Eu(L^{Me})$_2$(thf)$_2$]**), [Eu(*p*-HC$_6$F$_4$N(CH$_2$)$_2$NEt$_2$)$_2$(thf)$_2$] (**[Eu(L^{Et})$_2$(thf)$_2$]**), [Eu(*p*-HC$_6$F$_4$N(CH$_2$)$_2$NEt$_2$)$_2$(dme)] (**[Eu(L^{Et})$_2$(dme)]**) and [Yb(*p*-HC$_6$F$_4$N(CH$_2$)$_2$NEt)$_2$(dme)] ([Yb(L^{Et})$_2$(dme)]).[14]

	[Eu(L^{Me})$_2$(thf)$_2$]	**[Eu(L^{Et})$_2$(thf)$_2$]**	**[Eu(L^{Et})$_2$(dme)]**	[Yb(L^{Et})$_2$(dme)]
Ln(1)–N(1)	2.561(3)	2.561(17)	2.564(3)	2.428(3)
Ln(1)–N(3)	2.552(3)	2.536(14)	2.551(2)	2.436(3)
Ln(1)–N(2)	2.720(4)	2.823(17)	2.785(3)	2.729(3)
Ln(1)–N(4)	2.729(3)	2.796(18)	2.788(3)	2.728(3)
Ln(1)–O(1)	2.606(3)	2.650(15)	2.654(2)	2.560(3)
Ln(1)–O(2)	2.604(3)	2.622(13)	2.689(2)	2.588(3)
Ln(1)–F(1)	2.656(2)	2.683(10)	2.630(2)	2.558(2)
Ln(1)–F(5)	2.680(2)	2.679(10)	2.632(2)	2.560(2)

Structures of the homoleptic complexes [Eu(L^{Me})$_3$], [Sm(L^{Me})$_3$] and [Yb(L^{Et})$_3$]

The eight-coordinate homoleptic complexes **[Eu(L^{Me})$_3$]**, **[Sm(L^{Me})$_3$]** and **[Yb(L^{Et})$_3$]** crystallised in the space groups *P*−1, *P*−1 and *C*2/*c*, respectively. The molecular structure of **[Eu(L^{Me})$_3$]** is shown in Fig. 3, and the molecular structure of **[Yb(L^{Et})$_3$]** is shown in Fig. 4. Selected bond lengths for all complexes are listed in Table 2. In **[Eu(L^{Me})$_3$]** and **[Sm(L^{Me})$_3$]**, two of the amido ligands are tridentate (*N,N',F*), whereas the third ligand is only bidentate (*N,N'*), with the Ln–*o*-F(C) contacts non-bonding (≥ 3.753 Å).In contrast, complex **[Yb(L^{Et})$_3$]** features two tridentate (*N,N',F*) L^{Et} ligands but the third ligand has *N,F* coordination with an uncoordinated –

$(CH_2)_2NEt_2$ group. This represents an unusual case of linkage isomerism, and vividly highlights the lower steric demands of the L^{Me} ligand compared with the L^{Et} ligand. Coordination of the first two ligands results in less available coordination space for the third ligand in $[Ln(L^{Et})_3]$ than in $[Ln(L^{Me})_3]$ complexes, leading to the adoption of the less bulky *N,F* ligation. With reduction in size from NEt_2 to NMe_2, the metal atom in $[Ln(L^{Me})_3]$ is less crowded and can adopt the bulkier and evidently more stable chelating *N,N'* mode for the third ligand. In **$[Eu(L^{Me})_3]$**, both of the Eu–F(C) bond lengths are shorter than the corresponding Eu–NMe_2 bond lengths (Table 2). In the more sterically crowded **$[Yb(L^{Et})_3]$**, two of the Yb–F(C) bond lengths are shorter than the Yb–NEt_2 bond lengths, but the longest Yb–F(C) bond length (2.824(3) Å) is much longer than the other two Yb–F(C) bonds (2.413(2) and 2.501(2) Å). There are striking differences between $[Nd(L^{Et})_3]$ and the present ytterbium complex **$[Yb(L^{Et})_3]$**. Two of the Yb–F bonds are shortened by approximately 0.2 Å, well over the 0.12 Å expected,[31] whereas one is 0.19 Å longer, signalling a shift towards *N,N'* chelation for the tridentate N(1)/N(2)/F(1) ligand. Whilst the Ln–N(amide) bonds are shortened by at least the expected 0.12 Å, the Ln–NEt_2 bonds are only 0.07–0.08 Å shorter, indicative of weaker coordination of the neutral crowded nitrogen atoms in **$[Yb(L^{Et})_3]$**. Overall, ligand N(3)/N(4)/F(5) is readjusted in **$[Yb(L^{Et})_3]$** with a weaker Ln–NEt_2 bond and a much weaker Ln–F(C) interaction, whilst the other two ligands have stronger than expected Ln–F(C) binding. Thus, even though the formal connectivity of **$[Yb(L^{Et})_3]$** is the same as in $[Ln(L^{Et})_3]$ (Ln = La, Ce, Nd),[13] the Yb–*N',F* bond lengths are such that **$[Yb(L^{Et})_3]$** is quite different from the other three.

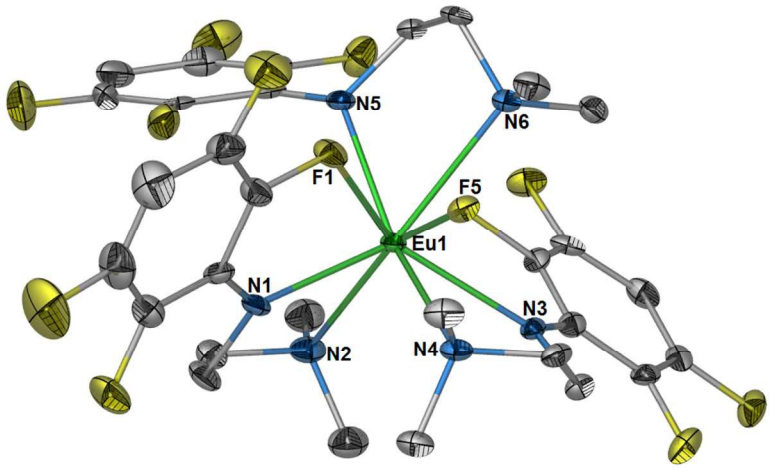

Fig. 3 Molecular structure of [Eu(*p*-$HC_6F_4N(CH_2)_2NMe_2)_3$] (**[Eu(L^{Me})$_3$]**) shown with 50 % probability thermal ellipsoids; hydrogen atoms have been omitted for clarity.

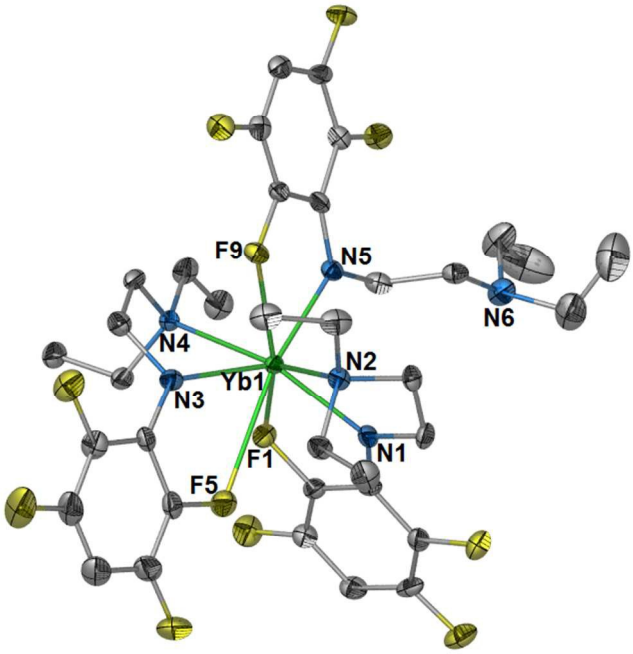

Fig. 4 Molecular structure of [Yb(*p*-$HC_6F_4N(CH_2)_2NEt_2)_2(thf)_2$] (**[Yb($L^{Et}$)$_3$]**) shown with 50 % probability thermal ellipsoids; hydrogen atoms have been omitted for clarity.

Table 2 Selected bond lengths (Å) for [Eu(*p*-$HC_6F_4N(CH_2)_2NMe_2)_3$] (**[Eu(L^{Me})$_3$]**), [Sm(*p*-$HC_6F_4N(CH_2)_2NMe_2)_3$] (**[Sm(L^{Me})$_3$]**) and [Yb(*p*-$HC_6F_4N(CH_2)_2NEt_2)_2(thf)_2$] (**[Yb($L^{Et}$)$_3$]**).

	[Eu(L^{Me})$_3$]	**[Sm(L^{Me})$_3$]**	**[Yb(L^{Et})$_3$]**
Ln(1)–N(1)	2.377(4)	2.388(2)	2.286(4)
Ln(1)–N(3)	2.448(4)	2.459(2)	2.242(4)
Ln(1)–N(5)	2.379(4)	2.383(2)	2.260(4)
Ln(1)–F(1)	2.552(3)	2.5619(17)	2.413(2)
Ln(1)–F(5)	2.590(3)	2.6050(17)	2.842(3)
Ln(1)–F(9)	—	—	2.501(2)
Ln(1)–N(2)	2.653(5)	2.662(2)	2.571(4)
Ln(1)–N(4)	2.695(4)	2.707(2)	2.636(4)
Ln(1)–N(6)	2.723(4)	2.744(2)	—

Structures of the iodo complexes [Eu(L^{Me})$_2$I(thf)] and [Yb(L^{Et})$_2$I]

In the iodo complexes **[Eu(L^{Me})$_2$I(thf)]** and **[Yb(L^{Et})$_2$I]**, which crystallised in the *P*−1 and *C*2/*c* space groups respectively, there is a decrease in coordination number from eight to seven accompanying the reduction in ionic radius from Eu^{3+} to Yb^{3+}, and the increase in steric bulk from L^{Me} to L^{Et}. The molecular structure of **[Eu(L^{Me})$_2$I(thf)]** is shown in Fig. 5 and the molecular structure of **[Yb(L^{Et})$_2$I]** is shown in Fig. 6. Selected bond lengths for both complexes are listed in Table 3. Both complexes have two tridentate (*N,N',F*) amide ligands and an iodide ligand, whilst **[Eu(L^{Me})$_2$I(thf)]** has an additional thf donor. Comparing the two iodo complexes, **[Eu(L^{Me})$_2$I(thf)]** and **[Yb(L^{Et})$_2$I]**, reveals one notable feature. For the ligand binding through N(1)/N(2)/F(1), the Ln–NR_2 bond length is only 0.04 Å shorter in the ytterbium complex than in **[Eu(L^{Me})$_2$I(thf)]**, indicating relatively weaker coordination in **[Yb(L^{Et})$_2$I]**, whilst Yb(1)–F(1) is 0.17 Å longer than Eu(1)–F(1), representing a much weaker bond. However, ligand N(3)/N(4)/F(5) behaves as expected for the difference in ionic radii. Overall, from Eu to Yb, one ligand partly detaches the F donor and the amine. Another feature is that the shortening of Ln–I from **[Eu(L^{Me})$_2$I(thf)]** to **[Yb(L^{Et})$_2$I]** greatly exceeds that expected,[31] presumably attributable to the much lower steric demand of iodide than the tridentate ligands. Overall, the change in Ln^{3+} size from **[Eu(L^{Me})$_2$I(thf)]** to **[Yb(L^{Et})$_2$I]** causes not just a reduction in coordination number but also a change in the attachment of one of the tridentate ligands.

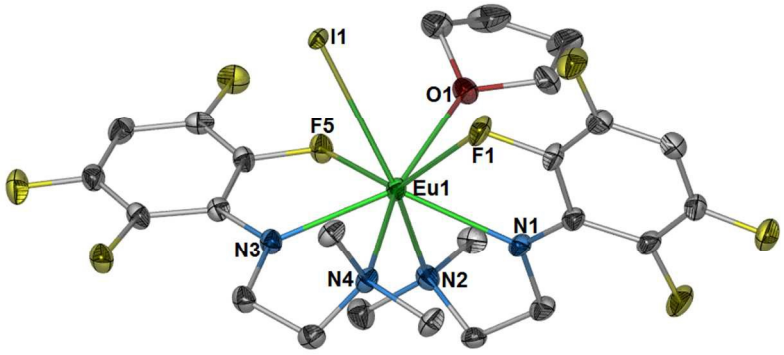

Fig. 5 Molecular structure of [Eu(*p*-$HC_6F_4N(CH_2)_2NMe_2)_2$I(thf)] (**[Eu(L^{Me})$_2$I(thf)]**) shown with 50 % probability thermal ellipsoids; hydrogen atoms have been omitted for clarity.

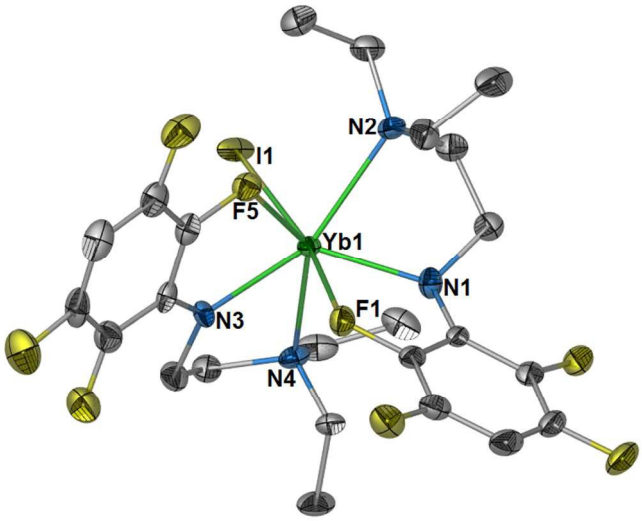

Fig. 6 Molecular structure of [Yb(*p*-$HC_6F_4N(CH_2)_2NMe_2)_2I$] (**[Yb(L^{Et})$_2$I]**) shown with 50 % probability thermal ellipsoids; hydrogen atoms have been omitted for clarity.

Table 3 Selected bond lengths (Å) for [Eu(*p*-$HC_6F_4N(CH_2)_2NMe_2)_2I$(thf)] (**[Eu(L^{Me})$_2$I(thf)]**) and [Yb(*p*-$HC_6F_4N(CH_2)_2NMe_2)_2I$] (**[Yb(L^{Et})$_2$I]**).

	[Eu(L^{Me})$_2$I(thf)]	**[Yb(L^{Et})$_2$I]**
Ln(1)–N(1)	2.400(3)	2.214(4)
Ln(1)–N(3)	2.390(3)	2.260(3)
Ln(1)–N(2)	2.597(3)	2.557(4)
Ln(1)–N(4)	2.595(3)	2.483(4)
Ln(1)–I(1)	3.1726(17)	2.928(4)
Ln(1)–F(1)	2.524(2)	2.713(3)
Ln(1)–F(5)	2.541(2)	2.374(3)
Ln(1)–O(1)	2.488(3)	—

Structures of the heteroleptic fluoride complexes [Sm(L^{Me})$_2$F]$_3$·1.5PhMe and [Sm(DippForm)(L^{Me})F]$_2$·2C_6H_6

The trinuclear heteroleptic samarium fluoride complex **[Sm(L^{Me})$_2$F]$_3$**·1.5PhMe crystallised in the *R*−3 space group and is isomorphous with the [Ln(L^{Me})$_2$F]$_3$·1.5PhMe (Ln = La, Ce) complexes,[13] whilst the dinuclear heteroleptic samarium fluoride complex **[Sm(DippForm)(L^{Me})F]$_2$**·2C_6H_6 crystallised in the monoclinic space group P2$_1$/*n*. The molecular structure of **[Sm(L^{Me})$_2$F]$_3$** is shown in Fig. 7, and the molecular structure of **[Sm(DippForm)(L^{Me})F]$_2$** is shown in Fig. 8.

Selected bond lengths for both complexes are listed in Table 4. As observed in other crystallographically characterised $[Ln(L^{Me})_2F]_3$ (Ln = La, Ce) complexes, **$[Sm(L^{Me})_2F]_3$** features three identical samarium atoms each coordinated by two tridentate (*N,N',F*) L^{Me} ligands (Sm–F(C) ca. 2.60 Å) and two bridging fluoride ligands. The distorted hexagonal $[Sm_3F_3]$ core is also seen in $[Sm\{Cp(tBu)_2\}F]_3$[32] and $[Ln(Cp)_2F]_3$ (Ln = Sc,[33] Yb[34]). In **$[Sm(DippForm)(L^{Me})F]_2$**, the tridentate *N,N',F* binding mode between the samarium atoms and the and L^{Me} ligands closely resembles that seen in **$[Sm(L^{Me})_2F]_3$**. Each formamidinate ligand chelates one samarium atom in a κ^2-*N,N'* manner, a common binding mode in other formamidinatosamarium halide complexes, e.g. $[Sm(DippForm)_2X(thf)]$ (X = F, Cl, Br, I).[35-37] Both samarium atoms are bridged by two fluoride ligands, forming a $[Sm_2F_2]$ core. A similar core has been seen previously in $[Nd(L^{Et})_2F]_2$.[13]

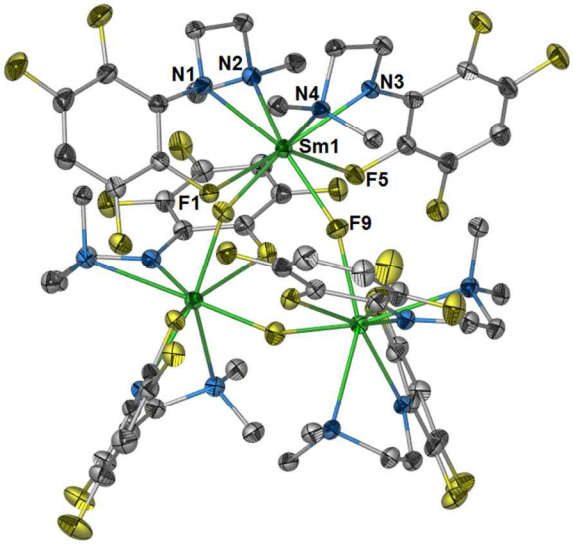

Fig. 7 Molecular structure of $[Sm(p\text{-}HC_6F_4N(CH_2)_2NMe_2)_2F]_3 \cdot 1.5PhMe$ (**$[Sm(L^{Me})_2F]_3$**·1.5PhMe) shown with 30 % probability thermal ellipsoids; hydrogen atoms and lattice solvent have been removed for clarity.

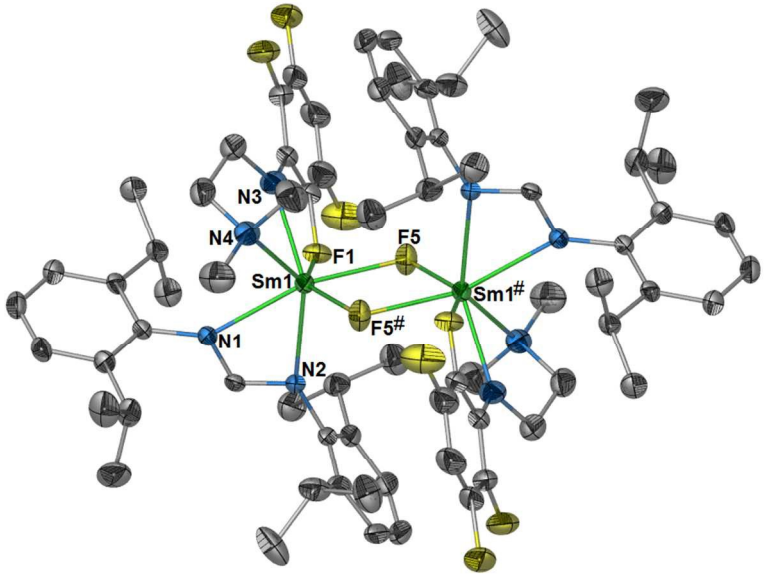

Fig. 8 Molecular structure of [Sm{2,6-(*i*Pr)$_2$C$_6$H$_3$NC(H)NC$_6$H$_3$(*i*Pr)$_2$-2,6}(*p*-HC$_6$F$_4$N(CH$_2$)$_2$NMe$_2$)F]$_2$·2C$_6$H$_6$ (**[Sm(DippForm)(L^{Me})F]$_2$**·2C$_6$H$_6$) shown with 50 % probability thermal ellipsoids; hydrogen atoms and lattice solvent have been removed for clarity.

Table 4 Selected bond lengths (Å) for [Sm(*p*-HC$_6$F$_4$N(CH$_2$)$_2$NMe$_2$)$_2$F]$_3$·1.5PhMe (**[Sm(L^{Me})$_2$F]$_3$**·1.5PhMe), [Sm{2,6-(*i*Pr)$_2$C$_6$H$_3$NC(H)NC$_6$H$_3$(*i*Pr)$_2$-2,6}(*p*-HC$_6$F$_4$N(CH$_2$)$_2$NMe$_2$)F]$_2$·2C$_6$H$_6$ (**[Sm(DippForm)(L^{Me})F]$_2$**·2C$_6$H$_6$) and [Eu$_4$(*p*-HC$_6$F$_4$N(CH$_2$)$_2$NEt$_2$)$_6$F$_2$O$_2$]·PhMe (**[Eu$_4$(L^{Et})$_6$F$_2$O$_2$]**·PhMe)

	[Sm(L^{Me})$_2$F]$_3$·1.5PhMe	**[Sm(DippForm)(L^{Me})F]$_2$** ·2C$_6$H$_6$	**[Eu$_4$(L^{Et})$_6$F$_2$O$_2$]**·PhMe	
			Eu(1)	Eu(2)
Ln–N(1)	2.427(5)	2.458(3)	2.487(5)	2.656(5)
Ln–N(3)	2.417(5)	2.375(4)	2.402(5)	—
Ln–N(5)	—	—	—	2.419(5)
Ln–N(2)	2.663(5)	2.488(3)	2.828(5)	—
Ln–N(4)	2.684(5)	2.558(4)	2.699(5)	—
Ln–N(6)				2.595(4)
Ln–F(1)	2.593(3)	2.553(2)	2.776(3)	—
Ln–F(5)	2.598(3)	2.261(2)	2.615(3)	—
Ln–F(5)$^{\#}$	—	2.289(2)	—	—
Ln–F(9)	2.250(4)	—	—	2.538(3)
Ln–F(9)$^{\#}$	2.254(4)	—	—	—
Ln–F(13)	—	—	2.282(3)	2.321(3)
Ln–O(1)	—	—	2.173(3)	2.176(3)
Ln–O(1)$^{\#}$	—	—	—	2.328(4)

Structure of $[Eu_4(L^{Et})_6F_2O_2]\cdot PhMe$

The tetranuclear europium complex, **$[Eu_4(L^{Et})_6F_2O_2]$**·PhMe, crystallised in the triclinic space group *P*−1. The structure is shown in Fig. 9, and bond lengths and angles are listed in Table 4. There are two europium environments. The first features two eight-coordinate Eu^{3+} ions, each bound by one tridentate (*N,N′,F*) L^{Et} ligand, one bridging (through the amide nitrogen) tridentate (*N,N′,F*) L^{Et} ligand, one bridging fluoride ligand and one bridging oxide ligand. The other europium environment features two seven-coordinate Eu^{3+} ions that are each bound to one tridentate (*N,N′,F*) L^{Et} ligand, one bridging monodentate (*N*) L^{Et} ligand, two bridging oxide ligands, and a bridging fluoride ligand. Although **$[Eu_4(L^{Et})_6F_2O_2]$** contains some short Eu–F(C) interactions, Eu–F(1) is noticeably elongated when compared with the Eu–F(C) bond lengths of **$[Eu(L^{Me})_2I(thf)]$** and **$[Eu(L^{Me})_2I(thf)]$** (see Table 2 and 3). This could be due to the presence of multiple hard fluoride and oxide ligands in **$[Eu_4(L^{Et})_6F_2O_2]$**.

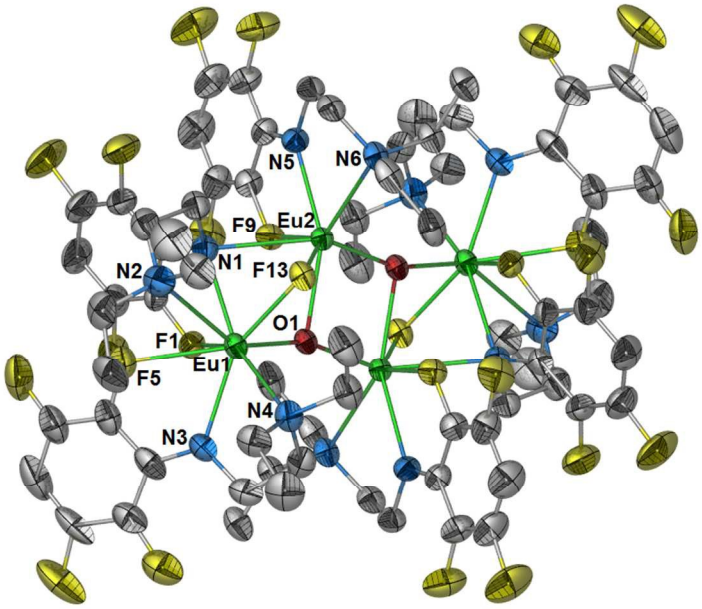

Fig. 9 Molecular structure of $[Eu_4(p\text{-}HC_6F_4N(CH_2)_2NEt_2)_6F_2O_2]\cdot PhMe$ (**$[Eu_4(L^{Et})_6F_2O_2]$**·PhMe) shown with 30 % probability thermal ellipsoids; lattice solvent and hydrogen atoms have been removed for clarity.

Insights into C–F activation

Our previous studies into C–F activation in the $L^{Me/Et}$ systems have shown that two and possibly even three C–F activation pathways are observed (Scheme 3; the third pathway is not included).[13, 14] In the first pathway, moderately stable Yb^{II} species are formed.[14] These complexes can then undergo radical fluoride abstraction involving oxidation of the Yb^{II} ions to Yb^{III} ions with concomitant reduction of the ligands. Multiple defluorination of the ligands was evidenced from GC/MS studies. The resulting Yb^{III} cage compounds, $[Yb_4(L^R)_6F_6]$, show a high F:Yb ratio (1.5:1). The second pathway involves lanthanoid metals without a stable divalent state.[13] In these instances, fluoride formation is believed to follow from fluoride abstraction and tetrafluorobenzyne formation from $[Ln(L^R)_2(C_6F_5)]$ intermediates in the RTP process. The resulting $[Ln(L^R)_2F]_n$ (Ln = La, Ce, R = Me, n = 3; Ln = Nd, R = Et, n = 2) complexes show a more modest F:Ln ratio of 1:1. The third pathway is more speculative but possibly involves oxidation of Ce^{III} to Ce^{IV}, and this was proposed to explain why heating a solution of $[Ce(L^{Me})_3]$ afforded $[Ce(L^{Me})_2F]_3$, in contrast to $[La(L^{Me})_3]$, which did not give $[La(L^{Me})_2F]_3$, even after prolonged heating.

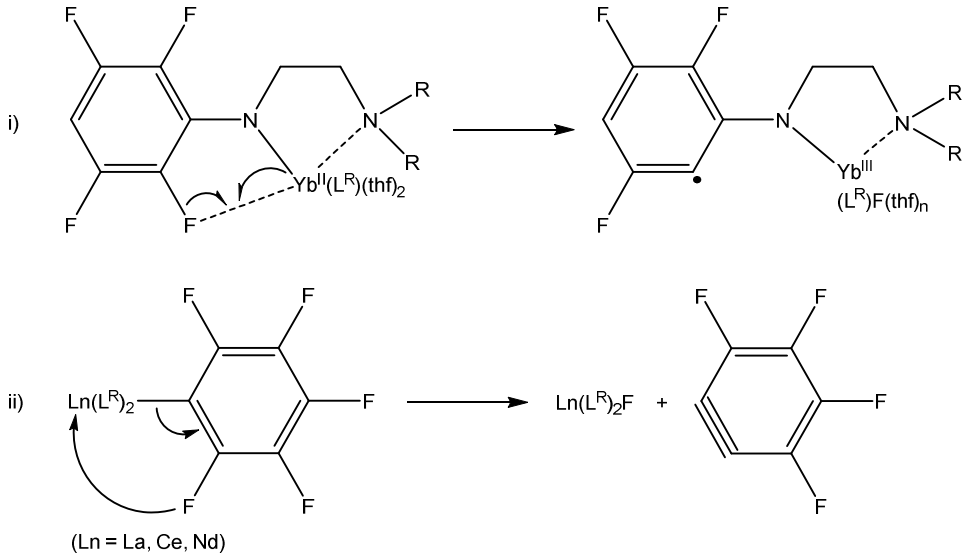

Scheme 3 The two main C–F activation pathways observed with the L^R ligand systems.

In the present study, we have investigated the effect of the stability of the divalent oxidation state on C–F activation by using lanthanoid metals with a divalent oxidation state more stable (Eu^{II}) than Yb^{II}, and and less stable than Yb^{II} (Sm^{II}). The Eu^{II} complexes show much higher thermal stability than the analogous Yb^{II} complexes and they require activation by light to promote C–F

cleavage. This phenomenon has been used to promote the reduction of perfluoroolefins by Ln^{II} complexes, and has been attributed to an enhanced reduction potential in the excited states.[1] Although we only isolated one Eu^{III} fluoride product, C–F activation can also be inferred from other key evidence. Firstly, GC/MS studies on a hydrolysed reaction mixture from a purple solution derived from activation of a solution of **[Eu(L^{Me})$_2$(thf)$_2$]** showed two organic species with *m*/*z* values of 218 and 434. The former corresponds to $[L^{Me}H - F + H]^+$. This has been observed before in the analogous Yb system. It is presumably derived from reduction and abstraction of a fluoride ion by the Eu^{II} ion to yield an organic radical, $[L^{Me}H - F]^\bullet$, which could then abstract a hydrogen from the solvent. The second species with an *m*/*z* value of 434 presumably derives from coupling of two $[L^{Me}H - F]^\bullet$ radicals before abstraction of hydrogen from the solvent can occur. Monitoring the C–F activation of a solution of **[Eu(L^{Et})$_2$(thf)$_2$]** by UV-vis spectroscopy (Fig. 10) showed that a new absorption band (λ_{max} = 513 nm) emerged as the colour gradually changed. Based on the absorption maximum observed for [Eu(L^{Me})$_2$I(thf)] (dark blue, λ_{max} = 613 nm), this can be tentatively assigned to a ligand→Eu^{III} charge transfer band. Residues obtained from activated solutions tested positive for fluoride (see Experimental for a reference to the method). The collective evidence supports the occurrence of C–F activation in the Eu^{II} systems but only a few single crystals of **[Eu$_4$(L^{Et})$_6$F$_2$O$_2$]** have been isolated to date.

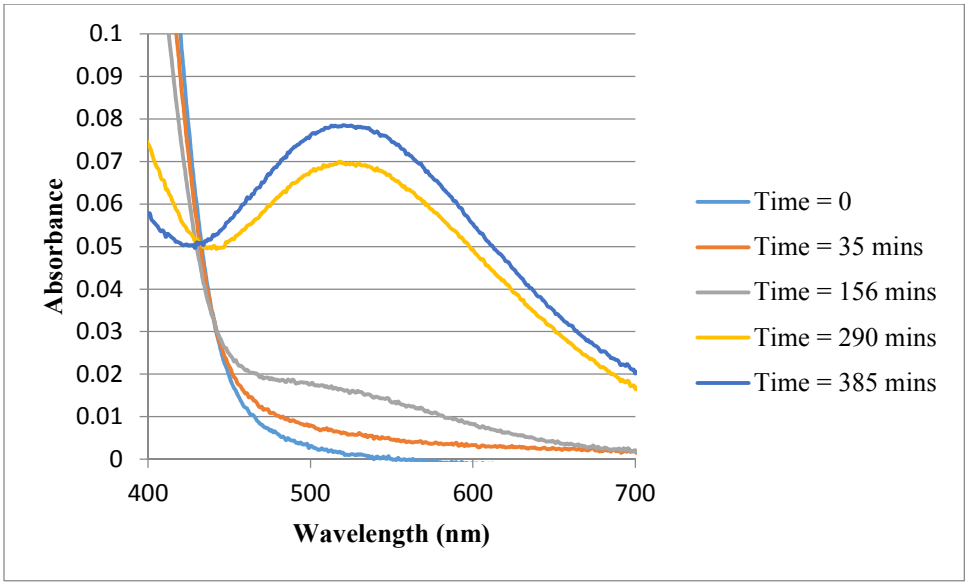

Fig. 10 Absorbance plot of **[Eu(L^{Et})$_2$(thf)$_2$]** in thf over time. The sample was enclosed in a box equipped with a halogen light source and the spectrum was periodically measured.

In contrast to the Eu^{II} systems, the highly reducing nature of the Sm^{II} ion meant that no divalent species were isolated. In fact, from an RTP reaction, only a handful of single crystals of **[Sm(L^{Me})$_2$F]$_3$**·1.5PhMe were isolated. This is probably due to the inherent instability of the transiently formed $Sm^{II}(C_6F_5)_2$, which has been shown to decompose into a variety of inorganic, organometallic and organic species.[38] In the present case, analysis of the hydrolysed reaction mixture by GC/MS was inconclusive. The bulk solid obtained from RTP reactions gave very low C, H and N analysis values, and this is suggestive of inorganic samarium fluoride products, possibly containing SmF_3. A qualitative inorganic fluoride test on this residue was positive (see Experimental). When we used the divalent precursor, [Sm(DippForm)$_2$(thf)$_2$], in order to attempt a protolysis reaction, once again no divalent intermediate was obtained and we only succeeded in isolating some single crystals of **[Sm(DippForm)(L^{Me})F]$_2$**·2C$_6$H$_6$ (Equation 2). Moreover, the failure of **[Sm(L^{Me})$_3$]** to yield any samarium fluoride products points to the importance of Sm^{II} in achieving C–F activation.

Thus, the highly reducing nature of Sm^{II} precludes attempts to effect control over C–F activation and the results are unpredictable. On the contrary, the reluctance of the Eu^{II} complexes to undergo C–F activation is the reason why well-defined C–F activation products were so difficult to obtain. Overall, the results show that for $L^{Me/Et}$ systems, Yb^{II} has the perfect balance between thermal stability of the divalent complexes and the reducing power of the Yb^{II} ion. This balance allowed for the isolation of trivalent heteroleptic fluoride complexes in high yields.[14] These observations are consistent with the standard $Ln^{3+} + e^- \rightarrow Ln^{2+}$ reduction potentials (−1.55 V, Ln = Sm; −1.15 V, Ln = Yb; −0.35 V, Ln = Eu).[18]

Conclusion

In summary, the effect of the stability of the divalent oxidation state of europium and samarium in C–F activation reactions with *N,N′*-dialkyl-2,3,4,5-tetrafluorophenyl-ethane-1,2-diaminate ligands (L^R; R = Me, Et) has been investigated. The divalent europium complexes, [Eu(L^R)$_2$(solv)$_2$] (R = Me, solv = thf; R = Et, solv = thf or $^1/_2$ dme), were synthesised by redox-transmetallation/protolysis (RTP). These complexes show good thermal stability but they undergo C–F activation if they are exposed to light, in one case yielding **[Eu$_4$(L^{Et})$_6$F$_2$O$_2$]**. Oxidation of [Ln(L^{Me})$_2$(thf)$_2$] (Ln = Eu, Yb) by I_2 yielded [Ln(L^{Me})$_3$] and [Ln(L^{Me})$_2$I(thf)$_n$] (Ln = Eu, n = 1; Ln = Yb, n = 0). Attempted transformation of **[Yb(L^{Et})$_2$I]** into **[Yb(L^{Et})$_3$]** failed

indicating that they are formed by two distinct pathways. The structure of **[Yb(L^{Et})$_3$]** differs markedly from those of reported [Ln(L^{Et})$_3$] (Ln = La, Ce, Nd) complexes in the pattern of bond lengths despite the same formal connectivity. A protolysis reaction between [Sm(CH$_2$C$_6$H$_4$-NMe$_2$-*o*)$_3$] and L^{Me}H afforded **[Sm(L^{Me})$_3$]**. **[Sm(L^{Me})$_3$]** is thermally robust and did not yield any samarium fluoride products after prolonged heating in toluene. An RTP reaction between Sm metal, Hg(C$_6$F$_5$)$_2$ and L^{Me}H gave a few single crystals of **[Sm(L^{Me})$_2$F]$_3$**·1.5PhMe, and a complex series of C–F activation reactions accounts for the failure to isolate further well-defined products in high yields. An attempted protolysis reaction between [Sm(DippForm)$_2$(thf)$_2$] with an excess of L^{Me}H afforded some single crystals of the C–F activation product **[Sm(DippForm)(L^{Me})F]$_2$**·2C$_6$H$_6$. Overall, the stability of the divalent oxidation state is crucial in determining the outcome of C–F activation reactions with L^R ligands. The stability of Eu^{II} impedes C–F activation, whilst the highly reducing nature of Sm^{II} leads to complex C–F activation reactions. Only Yb^{II} provides isolable divalent complexes that give well-defined C–F activation reactions.

Experimental

General: the compounds described herein were prepared and handled using conventional inert atmosphere techniques. IR spectra were recorded as Nujol mulls between NaCl plates using either a Perkin Elmer 1600 Series FTIR instrument or a Perkin Elmer Spectrum RX I FTIR Spectrometer within the range 4000–600 cm^{-1}. Multinuclear NMR spectra were recorded on a Bruker DPX 300 spectrometer. Chemical shifts were referenced to the residual ^{1}H resonances of the deuterated solvents (^{1}H) or external CCl$_3$F (^{19}F). UV-vis-NIR spectra were collected on a Cary 5G UV-Vis-NIR Spectrophotometer in a 1 mm quartz cell suitable for the handling of air- and moisture-sensitive materials. Melting points were determined in sealed glass capillaries under nitrogen and are uncalibrated. Microanalyses were determined by the Campbell Microanalytical Service, University of Otago (New Zealand), or the Elemental Analysis Service, London Metropolitan University. Metal analyses were determined by Na$_2$H$_2$edta titration following decomposition of the sample with HNO$_3$/H$_2$SO$_4$. GC/MS data were obtained with an Agilent 6890 series GC fitted with a 5% phenylmethylsiloxane capillary column (Agilent 19091S-433HP-5mS) interfaced to an Agilent 5987 network mass selective detector. Dme, hexane and thf were pre-dried over sodium metal and distilled over sodium benzophenone ketyl

before being stored under an atmosphere of nitrogen. Toluene, C_7D_8 and C_6D_6 were pre-dried over sodium and then distilled under nitrogen from sodium metal before being stored under an atmosphere of nitrogen. Absolute ethanol and methanol were used as received. Iodine was purchased from either Merck or Aldrich respectively and used as supplied. Lanthanoid metals were purchased from Santoku (America Int.) or Tianjiao (Baotou, China) as ingots, powders or rods and stored under nitrogen in a glove box. $Hg(C_6F_5)_2$,[39] *p*-$HC_6F_4NHC_2H_4NMe_2$ ($L^{Me}H$),[14, 40] *p*-$HC_6F_4NHC_2H_4NEt_2$ ($L^{Et}H$),[14] $[Yb(L^{Et})_2(thf)_2]$,[14] $[Sm(CH_2C_6H_4\text{-}NMe_2\text{-}o)_3]$[28] and $[Sm(DippForm)_2(thf)_2]$[35, 41] were prepared by literature methods. Inorganic fluoride was tested by following a general qualititative procedure as detailed by Vogel.[42]

Synthesis of [Eu(p-HC$_6$F$_4$N(CH$_2$)$_2$NMe$_2$)$_2$(thf)$_2$] ([Eu(L^{Me})$_2$(thf)$_2$])

Europium powder (0.46 g, 3.0 mmol), $Hg(C_6F_5)_2$ (0.80 g, 1.5 mmol), $L^{Me}H$ (0.71 g, 3.0 mmol) and one drop of Hg were stirred in thf (30 mL) for three days. The solvent was removed under vacuum and toluene (30 mL) was added. The mixture was filtered and the volume of the solution was concentrated under vacuum to 3 mL. Overnight storage (the flask was wrapped in aluminium foil to protect the contents from light) yielded **[Eu(L^{Me})$_2$(thf)$_2$]** as bright yellow crystals (0.62 g, 54 %). M.p. 166–170°C; (Found Eu 20.25; $C_{28}H_{38}EuF_8N_4O_2$ (766.58) requires Eu 19.82 %); IR (Nujol): ν = 1639 (vs), 1614 (sh), 1559 (s), 1526 (sh), 1498 (w), 1482 (vs), 1440 (sh), 1403 (w), 1354 (vs), 1295 (m), 1276 (m), 1250 (w), 1196 (w), 1147 (vs), 1138 (sh), 1060 (s), 1040 (vs), 957 (s), 921 (vs), 887 (m), 787 (w), 733 (m), 720 (sh), 690 (w), 668 (w), 648 (w), 626 (vw) cm^{-1}; $^{19}F\{^1H\}$ NMR (C_6D_6, 282.4 MHz, 303 K): −139.8 (br, s); T = 343 K: −138.4 (br, s). An NMR tube equipped with a J. Young valve was charged with **[Eu(L^{Me})$_2$(thf)$_2$]** (0.03 g) in CD_3CN (0.7 mL). One drop of trifluoroacetic acid was added and the tube was shaken. The ^1H NMR spectrum showed resonances attributable to thf and $L^{Me}H$ (integration 1:1).

GC/MS analyses of the decomposition of [Eu(L^{Me})$_2$(thf)$_2$]

A solution of **[Eu(L^{Me})$_2$(thf)$_2$]** in thf (0.5 mL) was placed under a halogen lamp for 6 h and the bright yellow colour changed gradually to purple. It was then hydrolysed with EtOH (two drops) and the insoluble materials were filtered off. The solution was then diluted with EtOH (0.5 mL). GC/MS: $R_t(m/z)$ = 11.740 (*m/z* 236) $[L^{Me}H]^+$, 12.855 (*m/z* 218) $[L^{Me}H - F + H]^+$, 13.295 (*m/z*

233) $[L^{Me}H - 3H]^+$, 18.101 (*m/z* 243), 23.068 (*m/z* 434) $[L^{Me}H - F]_2^+$, 23.777 (*m/z* 414) $[(L^{Me}H - F)_2 - HF]^+$.

Light-induced C–F activation of [Eu(L^{Me})$_2$(thf)$_2$]

As per the method above, **[Eu(L^{Me})$_2$(thf)$_2$]** was synthesised from europium powder (0.20 g, 1.3 mmol), $Hg(C_6F_5)_2$ (0.47 g, 0.88 mmol) and $L^{Me}H$ (0.42 g, 1.8 mmol). The solution was filtered and the solvent was removed under vacuum. Toluene (5 mL) was added and the solution was left exposed to light. The colour of the solution gradually changed from yellow to red/purple. Over the course of a week, some red/purple solid precipitated from solution. IR spectrum of dried solid (Nujol, cm^{-1}): 3367 (brw), 1644 (s), 1574 (m), 1500 (s), 1404 (w), 1355 (m), 1264 (s), 1210 (w), 1141 (s), 1099 (sh), 1059 (s), 1038 (s), 957 (m), 928 (s), 872 (w), 802 (s), 729 (w), 695 (w). The solid tested positive for fluoride.

Synthesis of [Eu(p-HC$_6$F$_4$N(CH$_2$)$_2$NEt$_2$)$_2$(thf)$_2$] ([Eu(L^{Et})$_2$(thf)$_2$])

Europium powder (0.91 g, 6.0 mmol), $Hg(C_6F_5)_2$ (1.60 g, 3.0 mmol), $L^{Et}H$ (1.59 g, 6.0 mmol) and one drop of Hg were stirred in thf (30 mL) for three days. The mixture was then filtered and the solution was concentrated under vacuum to 10 mL. The solution was then stored overnight at −30 °C yielding **[Eu(L^{Et})$_2$(thf)$_2$]** as bright yellow crystals (1.77 g, 72 %). M.p. 126–130°C; (Found C 43.35, H 5.09, N 7.04 (sample sent to New Zealand); $C_{26}H_{34}EuF_8N_4O_{0.5}$ (loss of 75 % thf, 714.53) requires C 43.70, H 4.80, N 7.84 %); (Found Eu 18.89 (freshly prepared sample); $C_{32}H_{46}EuF_8N_4O_2$ (822.68) requires Eu 18.47 %); IR (Nujol): *v* = 1640 (vs), 1556 (s), 1500 (vs), 1480 (vs), 1352 (s), 1298 (m), 1277 (w), 1244 (w), 1147 (vs), 1087 (w), 1068 (sh), 1054 (s), 1038 (s), 942 (s), 904 (w), 882 (w), 794 (w), 735 (m), 710 (m), 690 (w), 668 (w) cm^{-1}. The sample was hydrolysed in the same manner as **[Eu(L^{Me})$_2$(thf)$_2$]**. The ^{1}H NMR spectrum showed a thf:$L^{Et}H$ ratio of 1.6:2.0 (loss of 20 % thf).

C–F activation of [Eu(L^{Et})$_2$(thf)$_2$])

A solution of **[Eu(L^{Et})$_2$(thf)$_2$]** in thf was placed under a halogen light for 6 h and the bright yellow colour gradually changed to purple. UV-vis: λ_{max} = 518 nm.

Light-induced C–F activation of [Eu(L^{Et})$_2$(thf)$_2$]

As per the method above, **[Eu(L^{Et})$_2$(thf)$_2$]** was synthesised from europium powder (0.32 g, 1.3 mmol), $Hg(C_6F_5)_2$ (0.62 g, 1.2 mmol) and $L^{Et}H$ (0.62 g, 2.3 mmol). The solution was filtered and the solvent was removed under vacuum. Toluene (5 mL) was added and the solution was left exposed to light. The colour of the solution gradually changed to red/purple. Over time, some red/purple crystals precipitated from solution, along with a smaller number of orange crystals of **[Eu$_4$(L^{Et})$_6$F$_2$O$_2$]**, which were hand-picked for X-ray crystallography studies. The red/purple crystals were obtained on numerous occasions but they always diffracted very poorly. IR spectrum of dried mixture (Nujol, cm^{-1}): 3346 (brw), 1647 (s), 1574 (m), 1498 (s), 1296 (m), 1265 (w), 1208 (w), 1144 (s), 1062 (s), 947 (s), 910 (w), 796 (w). The mixture also tested positive for fluoride.

Synthesis of [Eu(p-HC$_6$F$_4$N(CH$_2$)$_2$NEt$_2$)$_2$(dme)] ([Eu(L^{Et})$_2$(dme)])

Dme (10 mL) was added to a Schlenk flask containing **[Eu(L^{Et})$_2$(thf)$_2$]** (1.22 g, 1.5 mmol). The solid dissolved with gentle heating forming a dark orange solution. The solution was then left to stand for 1 h after which time bright yellow crystals of **[Eu(L^{Et})$_2$(dme)]** deposited (0.53 g, 46 %). M.p. 178−184 °C; (Found C 42.30, H 5.20, N 7.34 (sample sent to New Zealand); $C_{24.67}H_{32.33}EuF_8N_4O_{0.67}$ (loss of 67 % dme, 699.50) requires C 42.35, H 4.66, N 8.01 %); (Found Eu 20.72 (freshly prepared sample); $C_{28}H_{40}EuF_8N_4O_2$ (768.59) requires Eu 19.77 %); IR (Nujol): ν = 1641 (s), 1556 (m), 1498 (m), 1351 (m), 1326 (w), 1297 (m), 1269 (w), 1244 (w), 1146 (m), 1058 (m), 1034 (w), 944 (m), 903 (m), 862 (m), 838 (w), 818 (w), 787 (m), 732 (s), 692 (m), 647 (w) cm^{-1}; $^{19}F\{^1H\}$ NMR (C_6D_6, 282.4 MHz, 303 K): −149.1 (br, s). The sample was hydrolysed in the same manner as **[Eu(L^{Me})$_2$(thf)$_2$]**. The ^1H NMR spectrum showed a dme:$L^{Et}H$ ratio of 1:2.

Synthesis of [Eu(p-HC$_6$F$_4$N(CH$_2$)$_2$NMe$_2$)$_2$I(thf)] ([Eu(L^{Me})$_2$I(thf)]) and [Eu(p-HC$_6$F$_4$N(CH$_2$)$_2$NMe$_2$)$_3$] ([Eu(L^{Me})$_3$])

A solution of I_2 (0.13 g, 0.50 mmol) in toluene (10 mL) was added to a solution of **[Eu(L^{Me})$_2$(thf)$_2$]** (0.77 g, 1.0 mmol) in toluene (10 mL) at ambient temperature. The solution was stirred for one hour and filtered. The volume of filtrate was reduced to 5 mL under vacuum. After standing overnight, blue rhombus crystals of **[Eu(L^{Me})$_2$I(thf)]** precipitated (0.61 g, 58 %). M.p. 145 °C (dec.); (Found C 33.80, H 3.50, N 6.95; $C_{22}H_{26}F_8IN_4O_{0.5}Eu$ (loss of 50 % thf, 785.33) requires C 33.65, H 3.34, N 7.13 %); IR (Nujol): ν = 1645 (m), 1573 (m), 1523 (w),

1492 (m), 1409 (w), 1397 (w), 1351 (m), 1299 (m), 1280 (m), 1153 (m), 1141 (s), 1078 (m), 1057 (m), 1041 (m), 1018 (m), 955 (m), 925 (s), 883 (w), 789 (m), 760 (w), 578 (w) cm^{-1}; ^1H NMR (C_6D_6, 300 MHz): could not be interpreted owing to paramagnetic shifting and broadening and a lack of meaningful integration at 303 or 343 K; $^{19}F\{^1H\}$ (C_6D_6, 282.4 MHz, 303 K): −139.6 (br, s; F3,5); T = 343 K: −139.2 (s, br, 4F; F3,5), −184.5 (s, $\Delta\upsilon_{1/2}$ = 1085 Hz, 4F; F2,6); UV-vis: λ_{max} = 613 nm , ε = 759 M^{-1} cm^{-1}; for the solid, λ_{max} = 609 nm. Further concentration of the remaining solution above led to the isolation of **[Eu(L^{Me})$_3$]** as a few bright blue crystals. The structure of **[Eu(L^{Me})$_3$]** was determined by X-ray crystallography. UV-vis: λ_{max} = 573 nm.

Synthesis of [Yb(p-HC$_6$F$_4$N(CH$_2$)$_2$NEt$_2$)$_2$I] ([Yb(L^{Et})$_2$I])

A solution of I_2 (0.13 g, 0.50 mmol) in toluene (10 mL) was added to a solution of **[Yb(L^{Et})$_2$(thf)$_2$]** (0.77 g, 1.0 mmol) in toluene (10 mL) at ambient temperature. The solution was stirred for one hour and filtered. The solvent was removed under vacuum and replaced with hexane (20 mL). The slurry was heated to obtain a dark orange solution. After standing for two days, dark red rhombus crystals of **[Yb(L^{Et})$_2$I]** precipitated (0.31 g, 38 %). M.p. 136–140 °C; (Found C 34.96, H 3.82, N 6.78; $C_{24}H_{30}F_8IN_4Yb$ (826.47) requires C 34.88, H 3.66, N 6.78 %); IR (Nujol): *v* = 1644 (m), 1581 (w), 1353 (m), 1302 (m) 1266 (w), 1208 (w), 1182 (w), 1151 (m), 1131 (w), 1059 (w), 996 (w), 944 (s), 909 (w), 875 (w), 812 (w), 790 (m), 767 (m), 690 (w), 667 (w), 658 (w) cm^{-1}; ^1H NMR (C_6D_6, 300 MHz, 343 K): −79.47 (s, 20H; Et), −31.44 (br, s, 4H; CH_2NEt_2), 9.55 (s, 4H; CH_2NAr), 21.81 (br, s, 2H; HC_6F_4); $^{19}F\{^1H\}$ NMR (C_6D_6, 282.4 MHz, 303 K): −127.5 (br, s; F3,5); T = 343 K: −35.3 (br, s, $\Delta\upsilon_{1/2}$ = 2799 Hz, 4F; F2,6), −130.8 (s, 4F; F3,5).

Synthesis of [Yb(p-HC$_6$F$_4$N(CH$_2$)$_2$NEt$_2$)$_3$] ([Yb(L^{Et})$_3$])

A solution of I_2 (0.10 g, 0.39 mmol) in toluene (5 mL) was added to a solution of [Yb(L^{Et})$_2$(thf)$_2$] (0.39 g, 0.46 mmol) in toluene (5 mL) at ambient temperature. The solution was stirred for one hour and filtered. The volume of the filtrate was reduced under vacuum to 2 mL and stored for three days, during which time red crystals of **[Yb(L^{Et})$_3$]** deposited (0.11 g, 34 %). M.p. 150–154 °C; (Found Yb 18.27; $C_{36}H_{45}F_{12}N_6Yb$ (962.82) requires Yb 17.97 %); IR (Nujol): *v* = 1644 (s), 1580 (s), 1495 (s), 1351 (s), 1298 (s), 1257 (m), 1207 (w), 1141 (s), 1062 (m), 995 (m), 945 (s), 911 (w), 878 (w), 791 (w), 761 (w), 733 (w), 690 (w), 657 (w), 614 (w) cm^{-1}; ^1H NMR (C_7D_8,

300 MHz, 343 K): −68.41 (br, s, 6H; CH_2NEt_2), −41.80 (br, s, 6H; CH_2NAr); 6.28 (br, s, 3H; HC_6F_4), 20.83 (br, s, 18H; Me), 26.82 (br, s, 12H; CH_2Me); T = 383 K: −59.20 (br, s, 6H; CH_2NEt_2), −32.73 (br, s, 6H; CH_2Ar), 6.98 (br, s, 3H; HC_6F_4), 18.02 (br, s, 18H; Me), 25.35 (br, s, 12H; CH_2Me); $^{19}F\{^1H\}$ NMR (C_7D_8, 282.4 MHz, 343 K): −134.8 (br, s); T = 383 K: −59.2 (vbr, s, 6F; F2,6), −135.8 (br, s, 6F; F3,5).

Synthesis of [Sm(p-HC$_6$F$_4$N(CH$_2$)$_2$NMe$_2$)$_2$F]$_3$ ([Sm(L^{Me})$_2$F]$_3$)

Samarium powder (0.37 g, 2.5 mmol), $Hg(C_6F_5)_2$ (0.42 g, 0.79 mmol) and $L^{Me}H$ (0.37 g, 1.6 mmol) were stirred in thf (10 mL) for one week at room temperature. The reaction mixture was filtered and then the solvent was removed under vacuum leaving a dark brown solid. Toluene (10 mL) was then added but not all of the solid dissolved. The solution was filtered into another Schlenk flask and the dark brown solid was dried under vacuum (0.31 g). (Found C 5.59 (bulk material), H 0.73, N 3.08; $C_{70.5}H_{78}F_{27}N_{12}Sm_3$ (2057.49) requires C 41.16, H 3.82, N 8.17 %); IR spectrum of dried solid (Nujol, cm^{-1}): 1643 (s), 1574 (m), 1500 (s), 1301 (s), 1262 (s), 1141 (s), 1058 and 1042 (s), 961 (m), 928 (m), 876 (w), 797 (w). GC/MS analysis of hydrolysed (performed in a similar manner to the europium(II) compounds) filtrate: R_t (min.): 9.02 (m/z = 298) $(C_{12}H_2F_8)^+$, 9.66 (m/z = 356), 10.68 (m/z = 341), 12.24 (m/z = 504), 13.66 (m/z = 364), 15.06 (m/z = 512), 15.40 (m/z = 411), 15.85 (m/z = 476), 17.66 (m/z = 620), 18.85 (m/z = 667), 19.32 (m/z = 627), 19.77 (m/z = 658), 20.15 (m/z = 672). The insoluble solid tested positive for fluoride. From a similar synthesis, some orange single crystals of **[Sm(L^{Me})$_2$F]$_3$**·1.5PhMe were hand-picked. Not enough pure material could be isolated for further analysis.

Synthesis of [Sm(p-HC$_6$F$_4$N(CH$_2$)$_2$NMe$_2$)$_3$] ([Sm(L^{Me})$_3$]$_2$)

$L^{Me}H$ (0.42 g, 1.8 mmol) was added at ambient temperature to a dark red solution of $[Sm(CH_2C_6H_4\text{-}NMe_2\text{-}o)_3]$ (0.27 g, 0.50 mmol) in toluene (10 mL). The mixture was stirred for three hours and the colour of the solution changed to light yellow. The solvent was removed under vacuum and the residue was washed with hexane (2 mL). The solid was dissolved in toluene (5 mL) and the volume of the solution was reduced to 1 mL under vacuum. The solution was stored overnight at ambient temperature, during which time light yellow crystalline **[Sm(L^{Me})$_3$]** formed. The solid was isolated and dried under vacuum (0.31 g, 72 %). M.p. 174–178 °C; (Found C 41.99, H 3.78, N 9.77; $C_{30}H_{33}F_{12}Sm$ requires (855.97): C 42.10, H 3.89, N

9.82 %); IR (Nujol): ν = 1646 (s), 1576 (m), 1495 (vs), 1379 (w), 1354 (w), 1283 (m), 1141 (s), 1047 (vs), 957 (m), 926 (vs), 873 (m), 791 (m), 776 (m), 719 (m) cm^{-1}; ^1H NMR (C_6D_6, 300 MHz, 333 K): −0.94 (s, 18H; Me_2N), 3.81 (s, 6H; CH_2NMe_2), 5.86 (br, s, 6H; CH_2NAr); 6.09 (t, ^3J = 9.6 Hz, 3H; HC_6F_4). $^{19}F\{^1H\}$ NMR (C_6D_6, 282.4 MHz, 333 K): −143.4 (s, 6F; F3,5), −164.8 (s, br, 6F; F2,6).

Attempted transformation of [Sm(L^{Me})$_3$] into [Sm(L^{Me})$_2$F]$_3$

A solution of **[Sm(L^{Me})$_3$]** (0.04 g) in C_7H_8 (0.7 mL) was heated at 110 °C for 72 h. No appreciable transformation of **[Sm(L^{Me})$_3$]** into **[Sm(L^{Me})$_2$F]$_3$** was detected by $^{19}F\{^1H\}$ NMR spectroscopy.

Synthesis of [Sm{2,6-(iPr)$_2$C$_6$H$_3$NC(H)NC$_6$H$_3$(iPr)$_2$-2,6}(p-HC$_6$F$_4$N(CH$_2$)$_2$NMe$_2$)F]$_2$·2C$_6$H$_6$ ([Sm(DippForm)(L^{Me})F]$_2$·2C$_6$H$_6$)

$L^{Me}H$ (0.028 g, 0.12 mmol) was added at ambient temperature to a green solution of [Sm(DippForm)$_2$(thf)$_2$] (0.030 g, 0.030 mmol) in C_6H_6 (0.7 mL), and the colour of the solution changed to light yellow after three minutes. The solution was stored for two days, during which time several light yellow crystals of **[Sm(DippForm)(L^{Me})F]$_2$**·2C_6H_6 formed.

X-ray diffraction structure determinations: Data collections were carried out at −150 °C (123 K) on a Bruker X8 APEX II CCD diffractometer for **[Eu(L^{Me})$_2$(thf)$_2$]**, **[Eu(L^{Et})$_2$(thf)$_2$]**, **[EuI(L^{Me})$_2$(thf)]**, **[Eu(L^{Me})$_3$]**, **[YbI(L^{Et})$_2$]**, or an Enraf-Nonius Kappa CCD diffractometer for **[Eu(L^{Et})$_2$(dme)]**, **[Yb(L^{Et})$_3$]**, and **[Li(L^{Et})]$_2$** (both diffractometers use graphite-monochromated Mo-K_α radiation (λ = 0.71073 Å)). The data for **[Sm(L^{Me})$_3$]**, **[Sm(L^{Me})$_2$F]$_3$**·1.5C_7H_8, and **[Sm(L^{Me})(DippForm)F]$_2$**·2C_6D_6 were collected at −173 °C (100 K) on the MX1 beamline at the Australian Synchrotron, Victoria, Australia, using Blu-Ice[43] and XDS[44] software. Each data set was empirically corrected for absorption (SORTAV[45] or SADABS[46]) then merged. The structures were solved by conventional methods and refined by full-matrix least-squares on all F^2 data using SHELXL-97 or SHELXL-2014,[47] in conjunction with the X-Seed[48] or Olex2[49] graphical user interfaces. All hydrogen atoms were placed in calculated positions using the riding model. Crystal data and refinement details are given in Table 5. CCDC-xxxxxx‑yyyyyy contains the supplementary crystallographic data for this paper. These data can be obtained free of charge from The Cambridge Crystallographic Data Centre via www.ccdc.cam.ac.uk/data_request/cif.

Table 5 Crystal data and structure refinement for complexes **[Eu(L^{Me})$_2$(thf)$_2$] – [Eu$_4$(L^{Et})$_6$F$_2$O$_2$]**·PhMe.

	[Eu(L^{Me})$_2$(thf)$_2$]	**[Eu(L^{Et})$_2$(thf)$_2$]**	**[Eu(L^{Et})$_2$(dme)]**	**[EuI(L^{Me})$_2$(thf)]**	**[Eu(L^{Me})$_3$]**	**[YbI(L^{Et})$_2$]**
formula	$C_{28}H_{38}F_8N_4O_2Eu$	$C_{32}H_{46}F_8N_4O_2Eu$	$C_{28}H_{40}F_8N_4O_2Eu$	$C_{24}H_{30}F_8N_4OIEu$	$C_{30}H_{33}F_{12}N_6Eu$	$C_{24}H_{30}F_8N_4IYb$
M_r	766.58	822.69	968.60	821.38	857.58	826.46
space group	$P2_1/c$	$P2_12_12_1$	$P2_1/n$	$P\bar{1}$	$P\bar{1}$	$P\bar{1}$
a, (Å)	10.1983(3)	13.2169(10)	12.435(3)	8.8112(2)	9.7220(4)	9.3478(3)
b, (Å)	18.4351(6)	16.1371(11)	18.083(4)	9.3315(2)	9.7602(2)	10.3678(3)
c, (Å)	16.4881(6)	33.290(3)	13.998(3)	17.4996(6)	17.8081(6)	14.5933(4)
α, (°)	90	90	90	99.446(2)	90.112(2)	79.421(2)
β, (°)	92.132(1)	90	90.39(3)	98.497(2)	104.966(2)	83.901(2)
γ, (°)	90	90	90	97.281(2)	98.250(2)	85.031(2)
V, (Å^3)	3097.73(18)	7100.1(9)	3147.5(11)	1386.85(6)	1614.23(11)	1379.16(7)
Z	4	8	4	2	2	2
μ, mm^{-1}	2.105	1.842	2.072	3.454	2.044	4.585
ρ_{calc}, g cm^{-3}	1.644	1.539	1.622	1.967	1.764	1.990
N_r	22577	48952	42568	20355	14823	21134
$N(R_{int})$	5318(0.0353)	16293(0.1602)	5542(0.056)	6385(0.0263)	5537(0.0564)	6310(0.0498)
$R1(I > 2\sigma(I))$	0.0296	0.0687	0.0325	0.0303	0.0416	0.0332
$wR2$(all data)	0.0774	0.1517	0.0989	0.0741	0.0961	0.0779
GOF	1.053	0.928	1.034	1.013	1.029	1.030

L' = 2,6-diisopropylphenylformamidinate

	[Yb(L^{Et})$_3$]	[Sm(L^{Me})$_3$]	[Sm(L^{Me})$_2$F]$_3$·1.5C_7H_8	[Sm(L^{Me})L'F]$_2$·2C_6D_6	[Eu_4(L^{Et})$_6F_2O_2$]·PhMe
formula	$C_{36}H_{45}F_{12}N_6Yb$	$C_{30}H_{33}F_{12}N_6Sm$	$C_{70.5}H_{78}F_{27}N_{12}Sm_3$	$C_{82}H_{104}F_{10}N_8Sm_2$	$C_{79}H_{98}F_{26}N_{12}O_2Eu_4$
M_r	962.82	855.97	2057.49	1692.49	2349.53
space group	*C*2/*c*	$P\bar{1}$	*R*-3	$P2_1/n$	$P\bar{1}$
a, (Å)	19.262(4)	9.7430(19)	22.323(3)	14.519(3)	11.610(2)
b, (Å)	13.409(3)	9.781(2)	22.323(3)	13.306(3)	12.902(3)
c, (Å)	30.044(4)	17.828(4)	53.058(11)	20.545(4)	15.759(3)
α, (°)	90	89.78(3)	90	90	90.19(3)
β, (°)	94.31(3)	75.07(3)	90	99.08(3)	91.45(3)
γ, (°)	90	81.69(3)	120	90	95.12(3)
V, (Å^3)	7738(3)	1623.4(6)	22897(8)	3919.4(14)	2350.4(8)
Z	8	2	12	2	1
μ, mm^{-1}	2.510	1.910	2.394	1.555	2.732
ρ_{calc}, g cm^{-3}	1.653	1.751	1.791	1.434	1.660
N_τ	28652	32234	118269	38015	55920
$N(R_{int})$	8747(0.0815)	6881(0.0595)	11581(0.0913)	8697(0.0853)	7745(0.0692)
$R1(I > 2\sigma(I))$	0.0420	0.0304	0.0540	0.0480	0.0457
*wR*2(all data)	0.1130	0.1517	0.1540	0.1181	0.1270
GOF	1.018	1.078	1.037	1.057	1.101

Acknowledgements

GBD and PCJ gratefully acknowledge the ARC for funding (DP130100152). RPK would like to thank the Faculty of Science for a Dean's Postgraduate Research Scholarship. Parts of this research were undertaken on the MX1: Macromolecular Crystallography beamline at the Australian Synchrotron, Victoria, Australia.

References

1. P. L. Watson, T. H. Tulip and I. Williams, *Organometallics*, 1990, **9**, 1999-2009.
2. H. Plenio, *ChemBioChem*, 2004, **5**, 650-655.

3. H. Plenio, *Chem. Rev.*, 1997, **97**, 3363-3384.
4. S. Banerjee, T. J. Emge and J. G. Brennan, *Inorg. Chem.*, 2004, **43**, 6307-6312.
5. J. H. Melman, T. J. Emge and J. G. Brennan, *Inorg. Chem.*, 2001, **40**, 1078-1081.
6. J. H. Melman, C. Rohde, T. J. Emge and J. G. Brennan, *Inorg. Chem.*, 2002, **41**, 28-33.
7. K. Norton, T. J. Emge and J. G. Brennan, *Inorg. Chem.*, 2007, **46**, 4060-4066.
8. H. Memmler, K. Walsh, L. H. Gade and J. W. Lauher, *Inorg. Chem.*, 1995, **34**, 4062-4068.
9. D. R. Click, B. L. Scott and J. G. Watkin, *Chem. Commun.*, 1999, 633-634.
10. L. Maron, E. L. Werkema, L. Perrin, O. Eisenstein and R. A. Andersen, *J. Am. Chem. Soc.*, 2005, **127**, 279-292.
11. I. Castillo and T. D. Tilley, *J. Am. Chem. Soc.*, 2001, **123**, 10526-10534.
12. H. Yin, A. J. Lewis, P. Carroll and E. J. Schelter, *Inorg. Chem.*, 2013, **52**, 8234-8243.
13. G. B. Deacon, C. M. Forsyth, P. C. Junk, R. P. Kelly, A. Urbatsch and J. Wang, *Dalton. Trans.*, 2012, **41**, 8624-8634.
14. G. B. Deacon, C. M. Forsyth, P. C. Junk and J. Wang, *Chem. Eur. J.*, 2009, **15**, 3082-3092.
15. F. Jaroschik, A. Momin, F. Nief, X.-F. Le Goff, G. B. Deacon and P. C. Junk, *Angew. Chem. Int. Ed.*, 2009, **48**, 1117-1121.
16. M. E. Fieser, M. R. MacDonald, B. T. Krull, J. E. Bates, J. W. Ziller, F. Furche and W. J. Evans, *J. Am. Chem. Soc.*, 2014, **137**, 369-382.
17. M. R. MacDonald, J. E. Bates, J. W. Ziller, F. Furche and W. J. Evans, *J. Am. Chem. Soc.*, 2013, **135**, 9857-9868.
18. W. J. Evans, *Inorg. Chem.*, 2007, **46**, 3435-3449.
19. M. N. Bochkarev, I. L. Fedushkin, A. A. Fagin, T. V. Petrovskaya, J. W. Ziller, R. N. R. Broomhall-Dillard and W. J. Evans, *Angew. Chem. Int. Ed.*, 1997, **36**, 133-135.
20. P. B. Hitchcock, M. F. Lappert, L. Maron and A. V. Protchenko, *Angew. Chem. Int. Ed.*, 2008, **47**, 1488-1491.
21. M. C. Cassani, D. J. Duncalf and M. F. Lappert, *J. Am. Chem. Soc.*, 1998, **120**, 12958-12959.
22. G. B. Deacon, P. C. Junk and R. P. Kelly, *Aust. J. Chem.*, 2013, **66**, 1288-1296.
23. J. L. Kiplinger, T. G. Richmond and C. E. Osterberg, *Chem. Rev.*, 1994, **94**, 373-431.

24. F. Alonso, I. P. Beletskaya and M. Yus, *Chem. Rev.*, 2002, **102**, 4009-4092.
25. M. Romanelli, G. A. Kumar, T. J. Emge, R. E. Riman and J. G. Brennan, *Angew. Chem.*, 2008, **120**, 6138-6140.
26. G. B. Deacon, F. Jaroschik, P. C. Junk and R. P. Kelly, *Chem. Commun.*, 2014, **50**, 10655-10657.
27. U. J. Williams, J. R. Robinson, A. J. Lewis, P. J. Carroll, P. J. Walsh and E. J. Schelter, *Inorg. Chem.*, 2014, **53**, 27-29.
28. C. Ruspic, J. R. Moss, M. Schürmann and S. Harder, *Angew. Chem. Int. Ed.*, 2008, **47**, 2121-2126.
29. G. B. Deacon, G. D. Fallon, C. M. Forsyth, H. Schumann and R. Weimann, *Chem. Ber.*, 1997, **130**, 409-415.
30. J. L. Atwood, W. E. Hunter, A. L. Wayda and W. J. Evans, *Inorg. Chem.*, 1981, **20**, 4115-4119.
31. R. D. Shannon, *Acta Cryst., Sect. A: Found. Crystallogr.*, 1976, **32**, 751-767.
32. H. Schumann, M. R. Keitsch, J. Winterfeld and J. Demtschuk, *J. Organomet. Chem.*, 1996, **525**, 279-281.
33. F. Bottomley, D. E. Paez and P. S. White, *J. Organomet. Chem.*, 1985, **291**, 35-41.
34. Glen B. Deacon, G. Meyer and D. Stellfeldt, *Eur. J. Inorg. Chem.*, 2000, **2000**, 1061-1071.
35. M. L. Cole, G. B. Deacon, P. C. Junk and K. Konstas, *Chem. Commun.*, 2005, 1581-1583.
36. M. L. Cole, G. B. Deacon, C. M. Forsyth, P. C. Junk, K. Konstas and J. Wang, *Chem. Eur. J.*, 2007, **13**, 8092-8110.
37. M. L. Cole, G. B. Deacon, P. C. Junk and J. Wang, *Organometallics*, 2013, **32**, 1370-1378.
38. G. B. Deacon, A. J. Koplick, W. D. Raverty and D. G. Vince, *J. Organomet. Chem.*, 1979, **182**, 121-141.
39. G. B. Deacon, C. M. Forsyth, D. L. Wilkinson and E. T. Lawrenz, in *Synthetic Methods of Organometallic and Inorganic Chemistry*, ed. F. T. Edelmann, Thieme, New York, 1997, vol. 6, pp. 48-51.

40. D. P. Buxton, G. B. Deacon, A. M. James, S. J. Knowles and T. L. Williams, *Polyhedron*, 1989, **8**, 2943-2945.
41. G. B. Deacon, P. C. Junk, J. Wang and D. Werner, *Inorg. Chem.*, 2014, **53**, 12553-12563.
42. A. I. Vogel, *A Text-Book of Qualitative Chemical Analysis Including Semimicro Qualitative Analysis*, Longmans, Green and Co. Ltd., London, 3rd edn., 1945, p. 271.
43. T. M. McPhillips, S. E. McPhillips, H.-J. Chiu, A. E. Cohen, A. M. Deacon, P. J. Ellis, E. Garman, A. Gonzalez, N. K. Sauter, R. P. Phizackerley, S. M. Soltis and P. Kuhn, *J. Synchrotron Rad.*, 2002, **9**, 401-406.
44. W. Kabsch, *J. Appl. Crystallogr.*, 1993, **26**, 795-800.
45. R. Blessing, *J. Appl. Crystallogr.*, 1997, **30**, 421-426.
46. G. M. Sheldrick, *SADABS: Program for Scaling and Absorption Correction of Area Detector Data*, Universität Göttingen, 1997.
47. G. Sheldrick, *Acta Cryst., Sect. A: Found. Crystallogr.*, 2008, **64**, 112-122.
48. L. J. Barbour, *J. Supramol. Chem.*, 2001, **1**, 189-191.
49. O. V. Dolomanov, L. J. Bourhis, R. J. Gildea, J. A. K. Howard and H. Puschmann, *J. Appl. Crystallogr.*, 2009, **42**, 339-341.

Table of contents entry

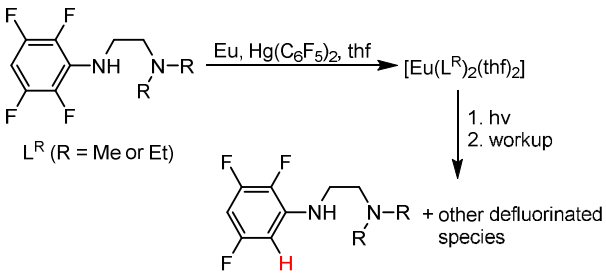

The role of the Ln^{II} oxidation state (Ln = Eu, Yb, Sm) in C–F activation reactions has been explored.